PHYSICAL REVIEW B **82**, 115427 (2010)

Flexural phonons and thermal transport in graphene

L. Lindsay,[1,2] D. A. Broido,[1] and Natalio Mingo[3,4]
[1]*Department of Physics, Boston College, Chestnut Hill, Massachusetts 02467, USA*
[2]*Department of Physics, Computer Science, and Engineering, Christopher Newport University, Newport News, Virginia 23606, USA*
[3]*CEA-Grenoble, 17 Rue des Martyrs, Grenoble 38000, France*
[4]*Department of Electrical Engineering, University of California, Santa Cruz, California 95064, USA*
(Received 6 July 2010; published 15 September 2010)

We show through an exact numerical solution of the phonon Boltzmann equation that the lattice thermal conductivity of graphene is dominated by contributions from the out-of-plane or flexural phonon modes, previously thought to be negligible. We connect this unexpected result to the anomalously large density of states of flexural phonons compared to their in-plane counterparts and to a symmetry-based selection rule that significantly restricts anharmonic phonon-phonon scattering of the flexural modes. The result is found to hold in the presence of the ripples known to occur in graphene, phonon-isotopic impurity scattering, and rigidity of the flexural phonon branch arising from the long-wavelength coupling between flexural and in-plane modes. Finally, accurate inclusion of the momentum conserving Normal phonon-phonon scattering processes within the context of a full solution of the phonon Boltzmann equation are shown to be essential in accurately describing the graphene thermal conductivity, in contrast to the more commonly used relaxation time and long wavelength approximations.

DOI: 10.1103/PhysRevB.82.115427 PACS number(s): 63.20.kg, 63.22.Rc, 66.70.−f, 65.80.Ck

I. INTRODUCTION

Since it was first exfoliated several years ago, graphene has been the subject of intense interest because of its unusual material properties and its potential for technological applications.[1–4] Its high carrier mobilities, room-temperature ballistic carrier transport,[1–4] and the observation of the quantum-Hall effect[5] reflect the high material quality and suggest possible use in future nanoelectronic devices.

Most of the research activity thus far has focused on the electronic properties of graphene while its thermal properties have been less studied. Recently, the phonon thermal conductivity of suspended graphene, κ_L, was measured using a novel Raman technique[6,7] and room-temperature values ranging from about 3000 W/m K to 5000 W/m K were recorded. These extremely high values are consistent with the high thermal conductivity of other carbon-based materials such as diamond,[8–10] graphite,[11] and single-walled carbon nanotubes (SWCNTs).[12,13]

Vibrations in the graphene lattice are characterized by two types of phonons: those vibrating in the plane of the layer with linear transverse and longitudinal acoustic branches (TA and LA), and those with vibrations out of the plane of the layer—the so-called flexural phonons (ZA and ZO). For many years it has been tacitly accepted that only in-plane acoustic phonons carry heat in graphene and the out-of-plane phonon contribution can be ignored.[14–17] This stemmed from the fact that the flexural acoustic (ZA) phonons have vanishing group velocities for wave vector, $\boldsymbol{q} \rightarrow 0$, and the connection made between large flexural mode Grüneisen parameters[18] and strong phonon-phonon Umklapp scattering.

Recently, we argued that, contrary to well-established belief, the ZA phonon modes in suspended graphene carry most of the heat.[19] We connected this unexpected result to the large density of modes for ZA flexural phonons resulting from their quadratic dispersion and to a selection rule for three-phonon scattering that arises from the reflection symmetry perpendicular to the graphene plane, and which strongly restricts the phase space for this scattering. Our theoretical result was found to be consistent with measurements of κ_L for graphene supported on SiO_2 substrates.[19]

In the present work, we provide a detailed account of our theoretical approach to describe phonon thermal transport in suspended graphene. This approach is based on an exact numerical solution of the linearized Boltzmann transport equation (BTE). In particular, it accurately incorporates the inelastic phonon-phonon scattering, which is primarily responsible for the thermal resistance. In the next section, we discuss two unique features that contribute to the anomalously large thermal conductivity of suspended graphene: (1) the large flexural phonon density of states and (2) the selection rule for anharmonic phonon scattering in two-dimensional (2D) layers, which we rigorously show is valid to all orders in the phonon-phonon scattering. The section following details the BTE approach to calculate κ_L. In Sec. IV, κ_L and its per branch contributions are presented as a function of temperature and of the length of the graphene sheet. The importance of the Normal phonon-phonon scattering processes in suspended graphene emerges from employing the full BTE solution, in contrast to the conventional relaxation-time approach. The commonly used[14–17,20–23] long wavelength approximation to the three-phonon scattering rates is shown to be of questionable validity, particularly for graphene. Also the effects on κ_L of the long wavelength renormalization of the flexural phonon branch arising from the coupling between in-plane and out-of-plane phonon modes is investigated,[24,25] as are the ripples known to occur in graphene.[26,27] Finally, we examine the reduction in κ_L due to phonon scattering by C^{13} isotopes.

II. DENSITY OF STATES AND SELECTION RULE

The ZA phonons in graphene have a quadratic dispersion over a wide range of the 2D Brillouin zone: $\omega_{ZA}(q)=\alpha_{ZA}q^2$, where α_{ZA} is a positive constant and $\boldsymbol{q}$ is the 2D phonon wave vector. The corresponding density of phonon modes, $D_{ZA}(\omega)=1/(4\pi\alpha_{ZA})$, is also constant. The mean number of phonons per unit ω about ω is $N(\omega)=n^0(\omega)D(\omega)$, where $n^0(\omega)$ is the Bose distribution function. Note that for $\omega\to 0$ $N_{ZA}(\omega)$ diverges as $1/\omega$. In contrast, the in-plane acoustic branches have linear dispersion, $\omega_{in}(q)\approx v_{in}q$ with $D_{in}(\omega)=\omega/2\pi v_{in}^2$, and, as $\omega\to 0$, $N_{in}(\omega)\to$ constant. Thus, the ratio, $N_{ZA}(\omega)/N_{in}(\omega)=v_{in}^2/2\alpha_{ZA}\omega$ diverges as $\omega\to 0$. Using accurately fit values for v_{TA} and α_{ZA} obtained from an optimized Tersoff empirical interatomic potential,[28,29] we find $N_{ZA}(\omega)/N_{TA}(\omega)\gg 1$ throughout the frequency range of ZA phonons, being about 9 at the ω corresponding to room temperature and still larger than 3 at the Brillouin zone boundary. For LA phonons, the corresponding ratios are even larger at about 20 and 7, respectively. Thus, for any temperature, the vast majority of thermally excited phonons come from the ZA branch. Furthermore, while the group velocities of ZA phonons are negligible, for very small q, they exceed 8000 m/s near the zone boundary, a speed more than half that of the TA phonons and far from negligible.

A selection rule on phonon-phonon scattering in flat graphene is revealed by examining the lattice potential energy, Φ, with respect to its equilibrium value

$$\Phi(\ldots\vec{r}_{\ell_i\kappa_i}\ldots)=\sum_{n=2}^{\infty}\frac{1}{n!}\sum_{\ell_1\kappa_1,\ldots,\ell_n\kappa_n}\sum_{\alpha_1,\ldots,\alpha_n}\Phi_{\alpha_1\ldots\alpha_n}(\ell_1\kappa_1;\ldots;\ell_n\kappa_n)u_{\alpha_1}(\ell_1\kappa_1)\cdots u_{\alpha_n}(\ell_n\kappa_n). \quad (1)$$

Here, $\vec{r}_{\ell\kappa}=\vec{R}_{\ell\kappa}+\vec{u}_{\ell\kappa}$ specifies the instantaneous location of the κth atom in the ℓth unit cell, and $\vec{R}_{\ell\kappa}$ and $\vec{u}_{\ell\kappa}$ give the equilibrium position and instantaneous displacement from equilibrium for that same atom. The nth order interatomic force constants (IFCs) are given by: $\Phi_{\alpha_1\ldots\alpha_n}(\ell_1\kappa_1;\ldots;\ell_n\kappa_n)=\frac{\partial^n\Phi}{\partial u_1(\ell_1\kappa_1),\ldots,\partial u_n(\ell_n\kappa_n)}\big|_0$, where the derivative is evaluated at the equilibrium lattice positions, as indicated by the vertical bar. The harmonic part in Eq. (1) corresponds to $n=2$; the remaining terms for $n\geq 3$ comprise the anharmonic part.

The potential must be invariant under the symmetry operations of the lattice. Equating like terms in the expanded potential before and after a symmetry operation yields a relation between nth order IFCs (Ref. 30)

$$\sum_{\alpha_1',\ldots,\alpha_n'}\Phi_{\alpha_1',\ldots,\alpha_n'}(\ell_1'\kappa_1';\ldots;\ell_n'\kappa_n')\Omega_{\alpha_1'\alpha_1}\cdots\Omega_{\alpha_n'\alpha_n}=\Phi_{\alpha_1,\ldots,\alpha_n}(\ell_1\kappa_1;\ldots;\ell_n\kappa_n). \quad (2)$$

Here, $\Omega_{\alpha\beta}$ are scalar elements of a general rotation matrix that can include inversion and the primes indicate the locations into which the corresponding unprimed positions are mapped by the transformation. For a 2D lattice in the xy plane, reflection about the z-axis maps the lattice into itself. Inserting the corresponding reflection matrix in Eq. (2) gives $\Phi_{\alpha_1,\ldots,\alpha_n}(\ell_1\kappa_1;\ldots;\ell_n\kappa_n)=(-1)^m\Phi_{\alpha_1,\ldots,\alpha_n}(\ell_1\kappa_1;\ldots;\ell_n\kappa_n)$, where m is the number of z components in the string, $\alpha_1,\ldots,\alpha_n$. For odd m, this can only be satisfied if

$$\Phi_{\alpha_1,\ldots,\alpha_n}(\ell_1\kappa_1;\ldots;\ell_n\kappa_n)=0,\quad m \text{ odd}. \quad (3)$$

In the harmonic approximation, Eq. (3) establishes a complete decoupling of in-plane and flexural phonons because of the vanishing of IFCs such as $\Phi_{xz}(\ell_1\kappa_1;\ell_2\kappa_2)$, as has been noted previously.[24,25,27] The anharmonic terms are also constrained by Eq. (3) to have only even numbers of z components in each nth order IFC. This results in the selection rule that *to all orders in anharmonic phonon-phonon scattering in 2D crystals such as graphene only even numbers (including zero) of flexural phonons can be involved.* Since phonon-phonon scattering provides the intrinsic thermal resistance, this selection rule has a profound effect on phonon thermal transport in graphene.

III. PHONON THERMAL TRANSPORT

To assess the significance of the large density of ZA phonon modes and of the selection rule, we calculate κ_L including only the third-order anharmonic term in the lattice potential, which is typically dominant. Phonon thermal transport is taken to occur across a graphene sheet having length, L, and infinite width perpendicular to the direction of transport. We have developed an exact numerical solution of the linearized 2D phonon BTE similar to that used previously for diamond crystal structures[31–33] and for SWCNTs (Ref. 34)

$$k_B T\boldsymbol{v}_\lambda\cdot\nabla T\frac{\partial n_\lambda^0}{\partial T}=\sum_{\lambda'\lambda''}\left[W^+_{\lambda\lambda'\lambda''}(\Psi_{\lambda''}-\Psi_{\lambda'}-\Psi_\lambda)+\frac{1}{2}W^-_{\lambda\lambda'\lambda''}(\Psi_{\lambda''}+\Psi_{\lambda'}-\Psi_\lambda)\right]-n_\lambda^0(n_\lambda^0+1)\Psi_\lambda\frac{1}{\tau_\lambda^{bs}}. \quad (4)$$

In Eq. (4), $\boldsymbol{v}_\lambda$ is the phonon velocity for mode $\lambda=j,\boldsymbol{q}$, where j is the phonon branch index, $n_\lambda^0=1/[\exp(\hbar\omega_\lambda\beta)-1]$ is the Bose distribution function with $\beta=1/k_BT$, and $\tau_\lambda^{bs}=L/2|v_{\lambda\alpha}|$ is a boundary scattering time (α indicates the component of

$\boldsymbol{v}_\lambda$ in the direction of heat flow) whose form has been chosen to recover both ballistic and diffusive limits for $L \to 0$ and $L \to \infty$, respectively.[35] The first term on the right-hand side (RHS) of Eq. (4) describes the inelastic anharmonic three-phonon scattering, which couples together the nonequilibrium phonon mode distributions, proportional to Ψ_λ. The sum is over the phase space of λ' and λ'' that satisfy momentum and energy ($\hbar\omega_\lambda$) conservation: $\boldsymbol{q} \pm \boldsymbol{q}' = \boldsymbol{q}'' + \boldsymbol{K}$, where $\boldsymbol{K}$ is a graphene reciprocal lattice vector and $\omega_j(\boldsymbol{q}) \pm \omega_{j'}(\boldsymbol{q}') = \omega_{j''}(\boldsymbol{q}'')$. This phase space is calculated on a fine grid throughout the Brillouin zone using the full graphene phonon dispersions, and it includes millions of Normal (N) and Umklapp (U) scattering processes. The three-phonon scattering rates, $W^{\pm}_{\lambda\lambda'\lambda''}$ describe "+" processes of the form $\lambda + \lambda' \leftrightarrow \lambda''$, and "−" processes, $\lambda \leftrightarrow \lambda' + \lambda''$.[31–34] They involve matrix elements, $\Phi^{\pm}_{\lambda\lambda'\lambda''}$, which give the strength of a three-phonon scattering event

$$\Phi^{\pm}_{\lambda\lambda'\lambda''} = \sum_{\kappa} \sum_{\ell'\kappa'} \sum_{\ell''\kappa''} \xi^{\pm}_{\lambda\lambda'\lambda''}(\kappa;\ell'\kappa';\ell''\kappa'') e^{i\boldsymbol{q}'\cdot\boldsymbol{R}_{\ell'}} e^{i\boldsymbol{q}''\cdot\boldsymbol{R}_{\ell''}}, \tag{5}$$

where

$$\xi^{\pm}_{\lambda\lambda'\lambda''}(\kappa;\ell'\kappa';\ell''\kappa'') = \sum_{\alpha\beta\gamma} \Phi_{\alpha\beta\gamma}(0\kappa,\ell'\kappa',\ell''\kappa'') \varepsilon^{\lambda}_{\alpha\kappa} \varepsilon^{\pm\lambda'}_{\beta\kappa'} \varepsilon^{-\lambda''}_{\gamma\kappa''},$$

α, β, γ are Cartesian components, the $\Phi_{\alpha\beta\gamma}(0\kappa, \ell'\kappa', \ell''\kappa'')$ are third-order anharmonic IFCs, and the $\varepsilon^{\lambda}_{\alpha\kappa}$ are phonon eigenvectors, with $\lambda \to -\lambda \Rightarrow \boldsymbol{q} \to -\boldsymbol{q}$. The harmonic and anharmonic IFCs necessary to calculate phonon frequencies, eigenvectors, and three-phonon scattering rates are obtained from an optimized Tersoff empirical interatomic potential,[28,29] which gives improved fits to the ZA, TA, and LA phonon branches.

Equation (4) is solved for the Ψ_λ using an iterative approach.[31–34] In zeroth order, the relaxation-time approximation (RTA) is obtained by setting $\Psi_{\lambda'}$ and $\Psi_{\lambda''}$ to zero allowing solution of $\Psi^{(0)}_\lambda$. Using $\Psi^{(0)}_\lambda$ on the RHS then allows determination of $\Psi^{(1)}_\lambda$. The iterative process is continued until convergence is achieved. The Ψ_λ can be related[31–34] to the scattering times for each mode, τ_λ, from which κ_L is obtained as $\kappa_L = \Sigma_j \kappa_j$ with the per-branch contributions given by

$$\kappa_j = \frac{k_B}{4\pi^2\delta} \int [\hbar\omega_j(\boldsymbol{q})\beta]^2 n^0[\omega_j(\boldsymbol{q})][n^0\omega_j(\boldsymbol{q})] + 1\} v_j^2(\boldsymbol{q}) \tau_j(\boldsymbol{q}) d\boldsymbol{q}. \tag{6}$$

Here, $\delta = 0.335$ nm is the thickness of the graphene layer.[36]

IV. RESULTS AND DISCUSSION

Figure 1 shows the calculated κ_L at $T = 300$ K, for phonon transport along the "armchair" direction as a function of L between 1 and 10 μm. Also shown are the corresponding contributions from the ZA, TA, and LA branches. The dominant contribution to κ_L comes from the ZA branch, which is greater than TA and LA contributions combined and is ~75% of κ_L at $L = 10$ μm. This unexpected result reflects in part the effect of the selection rule, which excludes all three-phonon processes having an odd number (one or three) of flexural phonons. Thus, for example, the following +processes cannot occur: ZA+ZA↔ZA, ZA+TA↔TA, ZA+TA↔LA, ZA+LA↔LA, ZA+ZA↔ZO, and ZA+ZO↔ZO. We find that about 60% of both the N and U three-phonon scattering phase space of ZA phonons is forbidden by the selection rule. The inset shows the contributions to each acoustic branch from Eq. (6) integrated up to frequency, ω, as a function of ω for the case $L = 10$ μm. The extended rise of the ZA curve over almost the full range of frequencies spanned by this branch shows that significant contributions to κ_{ZA} occur throughout the Brillouin zone.

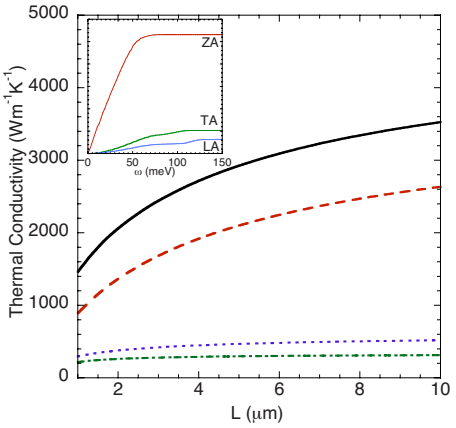

FIG. 1. (Color online) Calculated κ_L at $T = 300$ K as a function of the sheet length, L, along the transport direction (black solid curve). Also shown are κ_{ZA} (red dashed), κ_{TA} (blue dotted), and κ_{LA} (green dash-dotted) acoustic branches. Inset shows the total contribution to each branch as a function of phonon frequency. Units are also in W m^{-1} K^{-1}. Saturated values for large ω correspond to $\kappa_{ZA} \approx 2600$ W m^{-1} K^{-1}, $\kappa_{TA} \approx 520$ W m^{-1} K^{-1}, and $\kappa_{LA} \approx 315$ W m^{-1} K^{-1}.

The large density of flexural modes combined with their much smaller average frequencies ensures that their dominant contribution to κ_L will extend over a wide temperature range. Figure 2 illustrates this for $L = 10$ μm with plots of κ_{ZA}, κ_{TA}, κ_{LA}, and the combined contributions from the optic phonon branches as a function of temperature, T. The results are scaled by the total $\kappa_L(T)$, plotted as the black horizontal line. For large T, the contributions from ZA, TA, and LA branches approach a $1/T$ behavior characteristic of high temperature three-phonon scattering so their scaled values become horizontal to match the scaled $\kappa_L(T)$. For low temperatures, TA, LA, and optic phonons become frozen out and the scaled κ_{ZA} increases.

As pointed out above, ZA phonons with small ω are far more prevalent than those with large ω. As a result, N scattering of ZA phonons is unusually strong compared to U scattering. Since most materials have only linear acoustic branches, such behavior is typically seen only at low temperature, but for graphene it also occurs at much higher temperatures. The thermal conductivity obtained from the RTA solution of Eq. (4), κ_{RTA}, treats N scattering events as independent, resistive processes, which is physically incorrect since with only N scattering, κ_L must diverge,[37,38] a result

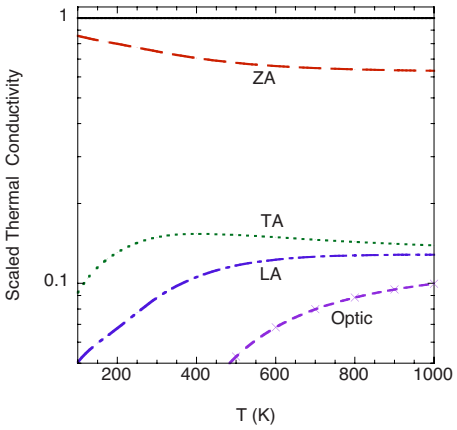

FIG. 2. (Color online) κ_{ZA} (red dashed), κ_{TA} (green dotted), and κ_{LA} (blue dash-dotted) and the combined contributions from the optic branches (dashed purple with crosses) as a function of temperature for $L=10$ μm. Values are scaled by $\kappa_L(T)$ (horizontal black line).

that is reproduced from our full calculations when U scattering and boundary scattering are removed. In most materials, corrections[38,39] to the RTA solution of the phonon BTE are typically small around room temperature because of strong U scattering. However, for graphene, κ_L lies considerably above κ_{RTA} as shown in Fig. 3, which plots the per branch contributions, κ_{ZA}, κ_{TA}, and κ_{LA} for $T=300$ K scaled by their corresponding RTA values as a function of L. Note that while the ZA branch shows the largest increase, κ_{TA} and κ_{LA} also lie well above their RTA values. This is because as the ZA phonon distribution function increases from its initial RTA values, the scattering channel, $ZA+ZA \rightarrow TA, LA$, causes the TA and LA distribution functions to also increase. The $-$ process: $TA, LA \rightarrow ZA+ZA$, maintains a balance between the distribution functions for the three branches.

Previous calculations of κ_L in graphene have used the long-wavelength approximation (LWA) to the three-phonon scattering rates.[14–17,20–23] The LWA is widely used in phonon transport models for both bulk and nanostructured systems. In the LWA, the solid is represented as an elastic continuum

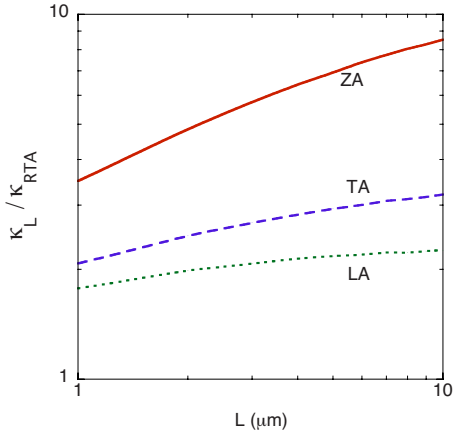

FIG. 3. (Color online) κ_{ZA} (solid red), κ_{TA} (blue dashed), and κ_{LA} (green dotted) for $T=300$ K and $L=10$ μm scaled by their corresponding RTA values.

with only acoustic branches included. The expressions for the three-phonon scattering matrix element in the LWA, $\Phi^{\pm}_{\lambda\lambda'\lambda''} \sim qq'q''$ implicitly assumes that the wave vectors q, q', and q'' of all three phonons involved in a scattering event are small. However, it is well known that three-phonon U scattering requires at least two phonons with large wave vector.[37] Thus, the small wave vector LWA assumption is, in principle, incompatible with the very U processes that provide the thermal resistance. Instead, one might expect the LWA to be appropriate only for low frequency N scattering. In fact, this has been confirmed from first-principles calculations,[39] which have shown that the accuracy of the LWA in silicon and germanium decreases rapidly with increasing phonon frequency. In any case, N scattering is typically not included in LWA models of phonon transport.[14–17,20–23] This exclusion is motivated by the notion that only U processes can provide thermal resistance. However, it ignores that fact that N processes provide the essential role of redistributing phonons to larger wave vectors so that U scattering can take place. In the context of graphene, we note finally that the LWA does not incorporate the symmetry of the three-phonon scattering matrix elements, $\Phi^{\pm}_{\lambda\lambda'\lambda''}$, from Eq. (5). As a result, it gives nonzero $\Phi^{\pm}_{\lambda\lambda'\lambda''}$ for *all* three-phonon scattering processes that satisfy momentum and energy conservation constraints *including the large fraction of these that must vanish because of the graphene selection rule*.

As noted in the second section above, the quadratic dispersion of the ZA branch causes $N_{ZA}(\omega) \sim 1/\omega$ as $\omega \rightarrow 0$. This produces a macroscopic divergence in the phonon density with system size.[40] It has been pointed out[24,25] that coupling between flexural and in-plane phonons renormalizes the long wavelength ZA dispersion, and recent calculations[25] have obtained this dispersion as $\omega_{ZA}(q)=\beta_{ZA}(q)q^2$ where $\beta_{ZA}(q)=\alpha_{ZA}[1+(q_c/q)^2]^{1/4}$ and q_c is a cut-off wave vector such that for $q \gg q_c$, the quadratic dispersion is recovered, but in the long-wavelength region, $q \ll q_c$, the graphene layer is stiffened such that $\omega_{ZA} \sim q^{3/2}$ which removes the divergence in the phonon density. We have incorporated the ZA dispersion from Ref. 25 into our calculations of κ_L. We find that doing so decreases κ_L by only about 1% for $L=10$ μm and $T=300$ K.[41] The smallness of this decrease is in part due to the fact that the boundary scattering has already effectively imposed a low-frequency cutoff on long-wavelength phonons.

We have also estimated the effect on the selection rule from the intrinsic ripples that occur in suspended graphene.[26,27] Using the amplitude and period of these ripples, we have estimated their curvature and determined from this an effective radius of a comparable SWCNT, which we find to be $\sim$29 nm. This corresponds to a $\sim(400,400)$ armchair SWCNT. Using our previously developed theory for SWCNTs,[34] we have calculated the strength of three-phonon processes that violate the graphene selection rule and find that at 29 nm radius, these are extremely weak. This suggests that the selection rule for flat graphene should also hold for graphene with ripples. On the other hand, in multilayer graphene and graphite the selection rule is broken by the weak interlayer coupling, which also creates a low-

lying optic phonon branch. We therefore expect a reduction in the κ_L for these systems compared to graphene.

We have also examined phonon scattering by isotopic impurities[31,33,34] by including 1.1% C^{13} in the C^{12} hexagonal lattice. We find a decrease in κ_L of $\sim 10-15$ % at room temperature over the range $L=1-10$ μm. We note that the resulting calculated value of $\kappa_L \sim 3000$ W/m K for $L=10$ μm is consistent with measured values for graphene flakes (see data point and error bars in Figs. 3 and 4 of Ref. 16). This is particularly noteworthy given that there are no adjustable parameters introduced in our thermal transport calculation.

While direct experimental verification of the large ZA contribution to κ_L is at present not available, recent measurements on graphene supported by SiO_2 substrates have been performed that show a reduction in κ_L.[19] These measurements can be explained by a substrate scattering model in which the ZA contribution to the κ_L for suspended graphene described in the present work is dominant. They are also consistent with strong breaking of the selection rule.

In connection with the above, it is straightforward to show that the phonon-phonon scattering selection rule for single-layer suspended graphene does not hold for multilayer graphene and graphite because of interlayer coupling. However, since this coupling is weak, one might expect that they will not strongly break the graphene selection rule. Another effect of the interplanar interactions in multilayer systems comes from the conversion of otherwise degenerate ZA phonon branches into low-lying optic branches whose contributions compared to the lone remaining ZA branch are reduced. A qualitatively similar effect should occur in single-walled carbon nanotubes, where the breaking of the reflection symmetry resulting from the nanotube curvature should enhance phonon-phonon scattering compared to that in suspended graphene.

V. SUMMARY AND CONCLUSIONS

Using an exact numerical solution to the phonon BTE, we have shown that flexural phonons provide the dominant contribution to the lattice thermal conductivity of suspended graphene. This finding is a consequence of: (1) the large density of flexural phonons associated with the quadratic ZA branch dispersion and (2) the reflection symmetry of two-dimensional graphene, which significantly restricts the phase space for phonon-phonon scattering of the flexural modes. The result holds for a wide range of graphene flake sizes and temperatures in the range of current experimental interest. It is also robust to inclusion of ripples, isotopic impurity scattering, and long-wavelength stiffness of the ZA branch produced by coupling between flexural and in-plane modes. Finally, the importance of including Normal phonon-phonon scattering in suspended graphene within the context of a full solution of the phonon BTE rather than using RTA or LWA approaches is highlighted.

ACKNOWLEDGMENT

The authors gratefully acknowledge support from the National Science Foundation under Grants No. CBET 0651381 and No. 0651310.

[1] K. S. Novoselov, A. K. Geim, S. V. Morozov, D. Jiang, Y. Zhang, S. V. Dubonos, I. V. Grigorieva, and A. A. Firsov, Science **306**, 666 (2004).
[2] K. S. Novoselov, D. Jiang, F. Schedin, T. J. Booth, V. V. Khotkevich, S. V. Morozov, and A. K. Geim, Proc. Natl. Acad. Sci. U.S.A. **102**, 10451 (2005).
[3] A. K. Geim and K. S. Novoselov, Nature Mater. **6**, 183 (2007).
[4] F. Schedin, A. K. Geim, S. V. Morozov, E. W. Hill, P. Blake, M. I. Katsnelson, and K. S. Novoselov, Nature Mater. **6**, 652 (2007).
[5] Y. Zhang, J. W. Tan, H. L. Störmer, and P. Kim, Nature (London) **438**, 201 (2005).
[6] A. A. Balandin, S. Ghosh, W. Bao, I. Calizo, D. Teweldebrhan, F. Miao, and C. N. Lau, Nano Lett. **8**, 902 (2008).
[7] S. Ghosh, I. Calizo, D. Teweldebrhan, E. P. Pokatilov, D. L. Nika, A. A. Balandin, W. Bao, F. Miao, and C. N. Lau, Appl. Phys. Lett. **92**, 151911 (2008).
[8] D. G. Onn, A. Witek, Y. Z. Qiu, T. R. Anthony, and W. F. Banholzer, Phys. Rev. Lett. **68**, 2806 (1992).
[9] J. R. Olson, R. O. Pohl, J. W. Vandersande, A. Zoltan, T. R. Anthony, and W. F. Banholzer, Phys. Rev. B **47**, 14850 (1993).
[10] L. Wei, P. K. Kuo, R. L. Thomas, T. R. Anthony, and W. F. Banholzer, Phys. Rev. Lett. **70**, 3764 (1993).
[11] G. A. Slack, Phys. Rev. **127**, 694 (1962).
[12] C. Yu, L. Shi, Z. Yao, D. Li, and A. Majumdar, Nano Lett. **5**, 1842 (2005).
[13] E. Pop, D. Mann, J. Cao, Q. Wang, K. Goodson, and H. Dai, Phys. Rev. Lett. **95**, 155505 (2005).
[14] P. G. Klemens, J. Wide Bandgap Mater. **7**, 332 (2000).
[15] P. G. Klemens, Int. J. Thermophys. **22**, 265 (2001).
[16] D. L. Nika, S. Ghosh, E. P. Pokatilov, and A. A. Balandin, Appl. Phys. Lett. **94**, 203103 (2009).
[17] D. L. Nika, E. P. Pokatilov, A. S. Askerov, and A. A. Balandin, Phys. Rev. B **79**, 155413 (2009).
[18] N. Mounet and N. Marzari, Phys. Rev. B **71**, 205214 (2005).
[19] J. H. Seol, I. Jo, A. L. Moore, L. Lindsay, Z. H. Aitken, M. T. Pettes, X. Li, Z. Yao, R. Huang, D. A. Broido, N. Mingo, R. S. Ruoff, and L. Shi, Science **328**, 213 (2010).
[20] P. G. Klemens, Solid State Phys. **7**, 1 (1958).
[21] B. D. Kong, S. Paul, M. B. Nardelli, and K. W. Kim, Phys. Rev. B **80**, 033406 (2009).
[22] A. Khitun and K. L. Wang, Appl. Phys. Lett. **79**, 851 (2001).
[23] Y. Gu and Y. Chen, Phys. Rev. B **76**, 134110 (2007).
[24] D. R. Nelson and L. Peliti, J. Phys. (Paris) **48**, 1085 (1987).
[25] E. Mariani and F. von Oppen, Phys. Rev. Lett. **100**, 076801 (2008).
[26] J. C. Meyer, A. K. Geim, M. I. Katsnelson, K. S. Novoselov, T. J. Booth, and S. Roth, Nature (London) **446**, 60 (2007).
[27] A. Fasolino, J. H. Los, and M. I. Katsnelson, Nature Mater. **6**, 858 (2007).
[28] J. Tersoff, Phys. Rev. Lett. **61**, 2879 (1988).
[29] L. Lindsay and D. A. Broido, Phys. Rev. B **81**, 205441

(2010).
[30] G. Leibfried and W. Ludwig, Solid State Phys. **12**, 275 (1961).
[31] M. Omini and A. Sparavigna, Nuovo Cimento D **19**, 1537 (1997).
[32] D. A. Broido, M. Malorny, G. Birner, and D. A. Stewart, Appl. Phys. Lett. **91**, 231922 (2007).
[33] A. Ward, D. A. Broido, D. A. Stewart, and G. Deinzer, Phys. Rev. B **80**, 125203 (2009).
[34] L. Lindsay, D. A. Broido, and N. Mingo, Phys. Rev. B **80**, 125407 (2009).
[35] N. Mingo and D. A. Broido, Nano Lett. **5**, 1221 (2005).
[36] A layer thickness is required to define the thermal conductivity. This value has conventionally been chosen to be 0.335 nm, the separation between graphene layers in graphite. We use it here in order to connect to previous work.
[37] J. M. Ziman, *Electrons and Phonons* (Oxford University Press, London, 1960).
[38] J. Callaway, Phys. Rev. **113**, 1046 (1959).
[39] A. Ward and D. A. Broido, Phys. Rev. B **81**, 085205 (2010).
[40] A. Geim, Science **324**, 1530 (2009).
[41] A bending rigidity of $\kappa_0=1.68$ eV was taken instead of $\kappa_0=1$ given in Refs. 25 and 27 in order to better fit the ZA dispersion for $q \gg q_c$. With this choice, we obtain $q_c \approx 0.15$ Å^{-1} about 1/10 of the distance to the Brillouin-zone boundary.